CO_2 migration and distribution in multiscale-heterogeneous deep saline aquifers

Ren, Jie; Wang, Yuan; Feng, Di; Gong, Jiakun

DOI
10.46690/ager.2021.03.08

Publication date
2021

Document Version
Final published version

Published in
Advances in Geo-Energy Research

Advances in Geo-Energy Research

Vol. 5, No. 3, p. 333-346, 2021

Original article

CO_2 migration and distribution in multiscale-heterogeneous deep saline aquifers

Jie Ren[1], Yuan Wang[2]*, Di Feng[3], Jiakun Gong[1,4]

[1]*College of Mechanics and Materials, Hohai University, Nanjing 210024, P. R. China*

[2]*College of Water Conservancy and Hydropower Engineering, Hohai University, Nanjing 210024, P. R. China*

[3]*College of Civil and Transportation Engineering, Hohai University, Nanjing 210024, P. R. China*

[4]*Department of Geoscience and Engineering, Delft University of Technology, Delft 2628CN, the Netherlands*

Keywords:
CO_2 migration and distribution
multi-scale
multi-facies
heterogeneous aquifers
transition probability
viscous fingering flow

Cited as:
Ren, J., Wang, Y., Feng, D., Gong, J. CO_2 migration and distribution in multiscale-heterogeneous deep saline aquifers. Advances in Geo-Energy Research, 2021, 5(3): 333-346, doi: 10.46690/ager.2021.03.08

Abstract:
Large volumes of carbon dioxide (CO_2) captured from carbon emission source can be stored in deep saline aquifers as a mean of mitigating climate change. The deep saline aquifers are naturally heterogeneous at multiple scales. It is important to generate representative multiscale heterogeneous fields of various hydrogeologic properties and understand storage safety by studying CO_2 migration and distribution in such fields. In this work, a new multiscale heterogeneous model with partly fine multi-facies heterogeneous domain is proposed. A method based on transition probability theory is referred to establish a multi-facies model. A new multiscale heterogeneous model with partly fine multi-facies heterogeneous domain is built up according to the categorized permeability data obtained from the Geological Carbon Storage Frio site in USA. TOUGH2/ECO2N is applied to simulate CO_2 migration and distribution in such a multiscale heterogeneous model. The CO_2 plume shows obvious viscous fingering and non-uniform migration both in layered and vertical directions, implying vertical and horizontal heterogeneity which cannot be represented by a single-scale model or simulated with the assumption of homogeneous formation. The profile of CO_2 migration shown in the numerical simulation at a time of 10 days is in a good accordance with the seismic data of Frio situ in qualitative and quantitative aspects.

1. Introduction

Carbon dioxide (CO_2) geological storage is an efficient way to alleviate global warming (IPCC, 2005; Soeder, 2021). Depleted oil and gas reservoirs, un-mineable coal seams, and deep saline aquifers are among the primary candidate formations for Geological Carbon Storage (GCS), and deep saline aquifers are currently recognized as the storage site with great storage potential (Bachu and Adams, 2003; Pacala and Socolow, 2004). Understanding of the migration and distribution of CO_2 in deep saline aquifers is the basis for ensuring the efficiency and safety of CO_2 storage.

Due to the discontinuity of the stratum deposition process, the deep saline aquifers are naturally heterogeneous (Koltermann et al., 1996; Slatt, 2006). Efforts have been made for evaluating CO_2 migration in heterogeneous deep saline aquifers located in various places: Kimberlina site in the Southwestern of California in USA (Birkholzer et al., 2009a, 2009b; Doughty et al., 2010), Frio site in Texas (Hovorka et al., 2004), In Salah site in Algeria (Cavanagh et al., 2011), Ketzin site in Germany (Ivandic et al., 2012), and Northern Quebec site in Canada (Teodoru et al., 2011). Heterogeneity of geologic reservoirs has profound effects on the migration of injected CO_2. Deng et al. (2012) proposed that heterogeneity in porosity and permeability of geologic reservoirs has a strong influence on CO_2 injection rate, CO_2 plume migration, storage capacity, potential leakage, and risk assessment. Conventional simulation methods based on the assumption of homogeneous formations (Nordbotten et al., 2005; Ronald et al., 2012; Oruganti et al., 2013; Raza et al., 2015) may lead to misevaluation of the storage efficiency and safety. How to characterize the heterogeneity of sedimentary

Yandy Scientific Press

*Corresponding author.
E-mail address: renjiehhu@163.com (J. Ren); wangyuanhhu@163.com (Y. Wang); fengdi@126.com (D. Feng); j.gong@tudelft.nl (J. Gong).

Received June 19, 2021; revised July 4, 2021; accepted July 5, 2021; available online July 10, 2021.

reservoirs is the key to study the law of CO_2 migration under the effect of heterogeneity.

The methods for characterizing reservoir heterogeneity can be roughly divided into two categories. One is to directly assign hydrogeological parameters to each unit in the simulation area through field drilling data. For example, Doughty (2010) matches the formation porosity and permeability parameters obtained on site to a numerical model to simulate the distribution characteristics of CO_2. Due to the limited drilling data on site, it is difficult to obtain measured parameters covering the entire study area. Therefore, a second method to characterize the formation heterogeneity is based on the on-site measured parameters, and the distribution field of global hydrogeological parameters is generated through random theory.

The porosity that characterizes the pore characteristics of storage media generally has the nature of volume average. The pore microstructure of underground porous rock formations can generally be reconstructed by log-normal distribution function number (Sahimi et al., 1991; Berkowitz et al., 1992; Sardini et al., 2006; Panja et al., 2021). Liu et al. (2010) apply log-normal distribution of random porosity to characterize the deep saline aquifer with heterogeneous structure in order to simulate the injection and distribution of carbon dioxide. Subsurface heterogeneity is controlled by the spatial variation of sedimentary facies types, facies are geometric features of rocks whose differentiation provides a useful framework to characterize heterogeneity (Soltanian et al., 2014). The commonly used method is to apply standard geophysical methods to generate random distributions of porosity or permeability, include a variogram approach using Sequential Indicator Simulation and a geo-statistical approach using Sequential Gaussian Simulation (Flett et al., 2007), random fields of log permeability are generated with the GSLIB software (Deutsch and Journel, 1998; Jahangiri et al., 2011; Basirat et al., 2016; Ren et al., 2018). The approach using transition probability based method has been adopted by many researches to create synthetic distributions of facies types, which provides a feasible way to represent the facies architecture using fundamental observable attributes such as volumetric proportion, mean lengths, and juxtaposition tendency (Carle, 1999). Doughty et al. (2004) uses transition probability theory to construct multiple two-dimensional stochastic representations of each depositional setting consistent with its idealized representation. Deng et al. (2012) develops a methodology that applies a transition probability based Markov chain model to generate facies-based heterogeneous fields of reservoir, and reveal the influence of reservoir heterogeneity on storage capacity, injection capacity, and leakage. The typical fluvial structure is well-captured by the transition-probability/Markov chain approach (Yang et al., 2020). Ershadnia et al. (2020) applies this method to simulate heterogeneous systems with binary facies distributions and the resulting petrophysical properties at the field scale, heterogeneous facies models are used to investigate the sensitivity of different trapping mechanisms as well as CO_2 plume dynamics to different variability.

However, the heterogeneous models based on transition probability theory mentioned above are mostly limited to single scale (mostly site-scale). The comprehensive assessment of CO_2 geological storage needs to calculate the coupling process at multi-scales. Middleton et al. (2012) defines the processes relevant at these scales: sub-pore scale (Å-10 nm), pore scale (10 nm-10 cm), CO_2 reservoir scale (10 cm-100 m), site scale (100 m-10 km), and region scale (10 km-1 Mm). Zhou et al. (2010) defines the plume scale (on the order of less than 100 km^2), and the basin scale (on the order of several 100,000 km^2). Recent studies have investigated the multi-scale conceptual models: Ramanathan et al. (2010) develops a geometric-based simulation methodology to model the hierarchical sedimentary architecture in braided channel belt deposits, the geologic model is a multi-scale complex representation of a fluvial architecture, which consists of several facies types spanning from the cm to the hundred meter scale (Soltanian et al., 2017). A number of recent studies adapte the method of Ramanathan et al. (2010) to create conceptual and quantitative models for sedimentary architecture in fluvial deposits over a range of scales that are relevant to CO_2 injection and storage. These studies cover several trapping mechanisms that control the fate and transport of injected CO_2. Gershenzon et al. (2015, 2017a) adapt this method investigate capillary trapping in heterogeneous fluvial-type reservoirs, and show that snap-off trapping exists in heterogeneous reservoirs even during the injection period. Soltanian et al. (2017) perform simulations of three-dimensional (3D) heterogeneous formations, which focus on the importance of facies-based heterogeneity and connectivity on advection-diffusion transport of dissolved CO_2. Gershenzon et al. (2017b) analyze the sensitivity of capillary trapping and dissolution to the variability in basic petrophysical parameters and rock composition in highly heterogeneous fluvial-type reservoirs. More comprehensively, Soltanian et al. (2019) conducts detailed numerical simulation studies that consider advection, dispersion, geo-mechanic, dissolution, convective mixing, and reaction coupled processes in fluvial depositional system. It is worth noting that the grid-cell size is defined by the characteristic size of the smallest scale facies types in this multi-scale heterogeneous model, since larger grid-cell sizes cannot capture the small-scale heterogeneities. Therefore, there is a trade-off between the grid-cell size and the domain size to make the problem computationally feasible (Soltanian et al., 2017).

In this study, an approach that applies the transition probability based Markov chain model is developed to generate facies-based multiscale heterogeneous model (Section 2). In the following sections, a multi-phase flow simulations in the Frio brine pilot is presented in Section 3. The simulation results is described in Section 4, while the conclusion is presented in Section 5.

2. Methodology

2.1 Heterogeneity model

We use the Transition Probability Geostatistical Software (T-PROGS) developed by Lawrence Livermore National Laboratory to establish a random multi-facies heterogeneous structure feature model (Carle, 1999). The software is based on the delay theory and takes into account the spatial cross-

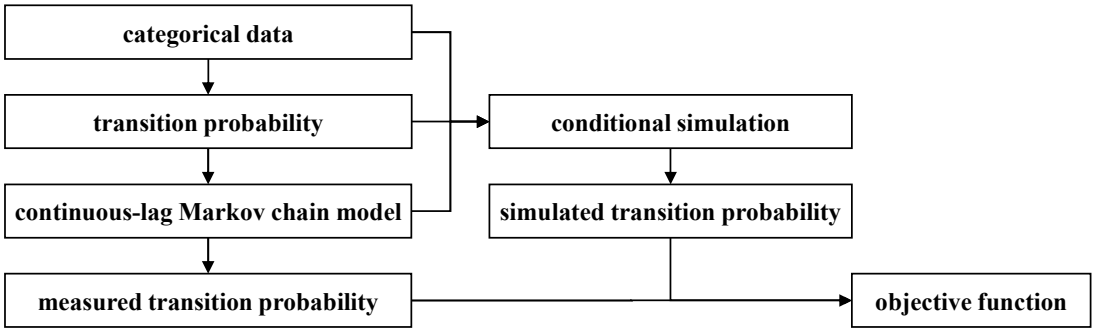

Fig. 1. The generation process of random multi-facies heterogeneous model.

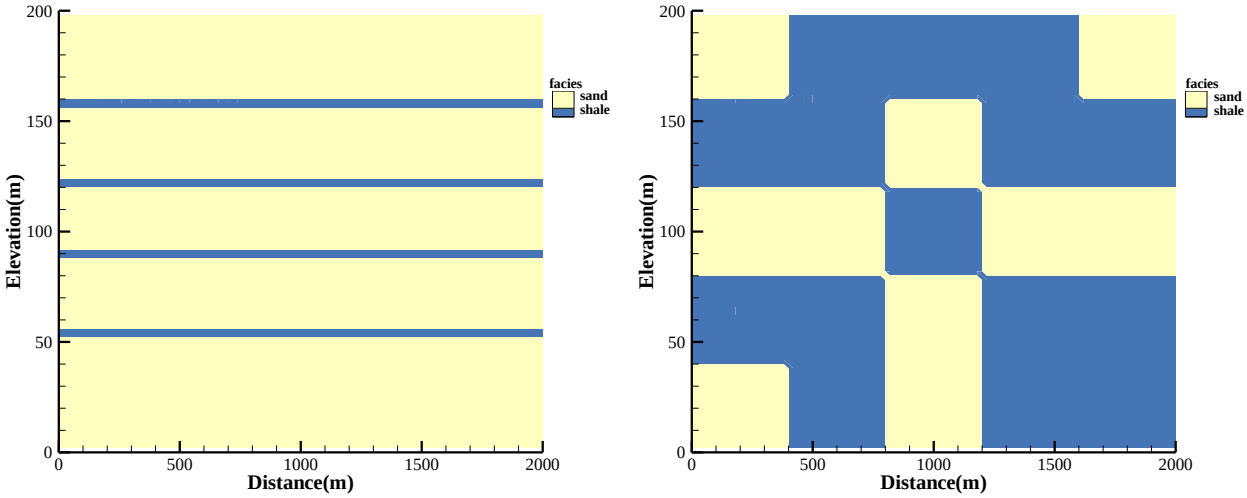

Fig. 2. Single-scale heterogeneity models, (a) single-scale interlayer heterogeneity model, (b) single-scale multi-facies heterogeneity model.

correlation of geological bodies which lead to more reproducible performance process. As shown in Fig. 1, typically, there are four steps to build up a random multi-facies heterogeneous model.

Firstly, categorize the given data of hydrogeologic parameter and compute the transition probabilities. (1) Set a value of lag or spatial dependency and relative thicknesses of the facies. (2) Record the succession of facies occurrences under a lag Δh_z. (3) Tally up the transition rate matrix. (4) Divide each row by the row sum to obtain the transition probability.

Secondly, develop the continuous-lag Markov chain models (Carle, 1999) and obtain the measured transition probabilities of all grid blocks. (5) Obtain different transition probability matrix as a discrete-lag form with different lag Δh_z. (6) Convert the discrete-lag form to the continuous-lag form by computing the transition rate matrix. (7) Obtain the 3D continuous-lag Markov chain model.

Thirdly, generate simulated transition probabilities along a random path of all grid blocks using the sequential indicator simulation algorithm (Deutsch and Journel, 1998). (8) Generate a random path through all centers of grid blocks. (9) Calculate conditional probabilities with given data and put them into a collection. Start from the first center of grid block in the random path. Compute the local conditional probability by formula (7), which is simulated transition probability when facies k occurs at the first grid block. (10) Add the new simulated value to the conditional probabilities collection. Compute the local conditional probability of the second center of grid block in the random path. Repeat cycle along the random path until local conditional probability of each grid block is obtained.

Finally, minimize the objective function by applying the simulated quenching algorithm (Carle, 1999) and obtain the optimum facies for each grid block.

2.2 Multi-scale multi-facies heterogeneous model

In the study of site-scale carbon dioxide storage, the establishment of a complete heterogeneous structure model has higher requirements for on-site measurement data. We propose that under the condition of limited data, in order to make the established model as close as possible to the characteristics of on-site stratigraphic distribution, the local important regions of single-scale interlayer heterogeneity or multi-facies heterogeneity (Fig. 2) can be further subdivided, thus the multi-scale multi-facies heterogeneity structure model can be obtained. According to site hydrogeologic characterization, three multi-scale heterogeneity models can be established: (a) multi-layered heterogeneous model including multi-facies

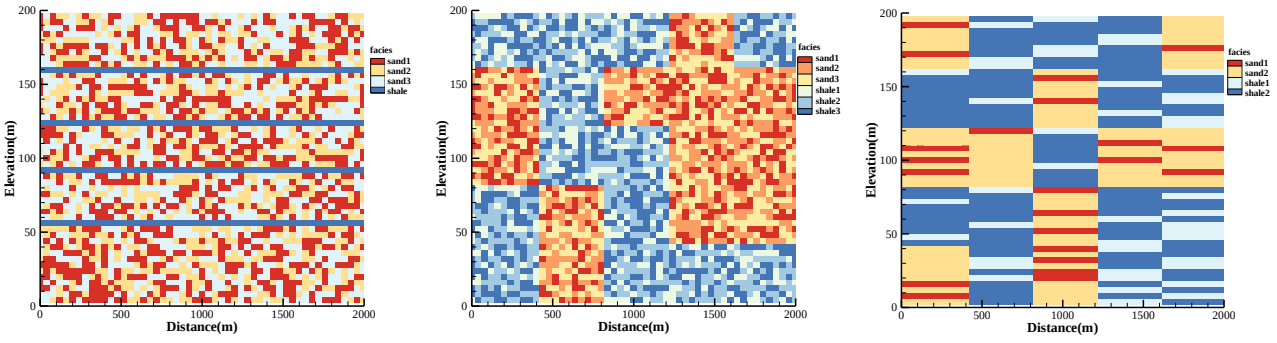

Fig. 3. Three types of multi-scale heterogeneity models, (a) multi-layered heterogeneous model including multi-facies heterogeneous model, (b) multi-facies heterogeneous model including multi-facies heterogeneous model, (c) multi-facies heterogeneous model including multi-layered heterogeneous model.

heterogeneous model, (b) multi-facies heterogeneous model including multi-facies heterogeneous model, and (c) multi-facies heterogeneous model including multi-layered heterogeneous model (as shown in Fig. 3).

3. Multi-phase flow simulations in Frio Brine Pilot

A multiscale heterogeneous model with partly fine multi-facies heterogeneous domain is built up with parameters obtained from the CCS pilot site in Frio, USA. The Frio project is located in the southeastern part of Houston, Texas, USA, close to most carbon dioxide emission sources. In 2004, the Frio I pilot program conducted the first CO_2 injection of about 1,600 tons in 10 days, which was carried out into the upper C-sand of the Frio Formation at a depth of 1,528.5-1,534.7 m (Hovorka et al., 2006).

3.1 Rock properties

The Frio saline aquifer has a thickness of about 60 m and a dip of about 18°. In the vertical direction, it shows a multi-layer structure with a sandstone layer A (8 m), a clay layer (6 m), a sandstone layer B (12 m), a clay layer (10 m) and a sandstone layer C (24 m) from top to bottom, the sandstone layer C is the target storage layer for CO_2. In each layer, a multi-facies structure with an uncertain spatial distribution of porosity and permeability is presented. The injection well locates at the top of the sandstone layer C with a length of 5.5 m. Fig. 4 shows the vertical layered structure of the Frio site. Fig. 5 shows the porosity and permeability in the sandstone layer C. Fig. 6 presents the capillary pressure curves measured in sandstone and clay.

At the Frio site, the porosity of sandstones ranges from 0.23 to 0.35, and the permeability of sandstones ranges from 0.2 to 3.7 D ($1\ \mathrm{D} = 1 \times 10^{-12}\ \mathrm{m}^2$) . The averaged porosity and permeability of clay are 0.14 and 0.001 D, respectively. According to these properties, the four-facies formation can be divided into more facies. As a result, a multiscale heterogeneous model can be established.

3.2 Frio multiscale heterogeneous model

The Frio multiscale heterogeneous model can be obtained by inserting random multi-facies models of special domain into a multilayer model (as show in Fig. 3(a)). This model has a dimension of 800 m × 400 m × 60 m containing a 200 m × 200 m × 16.5 m partly fine multi-facies heterogeneous domain (as shown in Fig. 7). The multiscale and multi-facies heterogeneous 3D model is divided into 70,000 units. Along

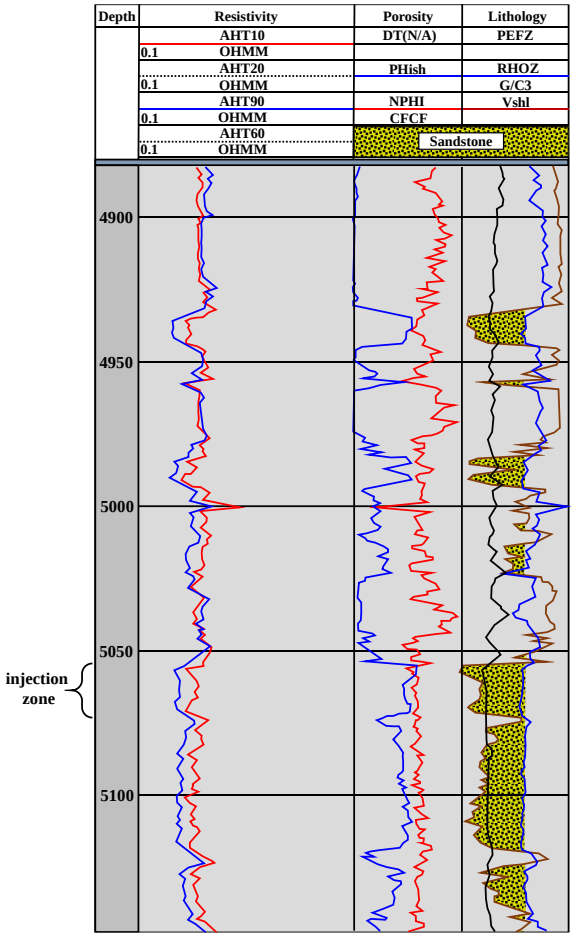

Fig. 4. Vertical layered structure of Frio site (modified from Kharaka et al. (2009)).

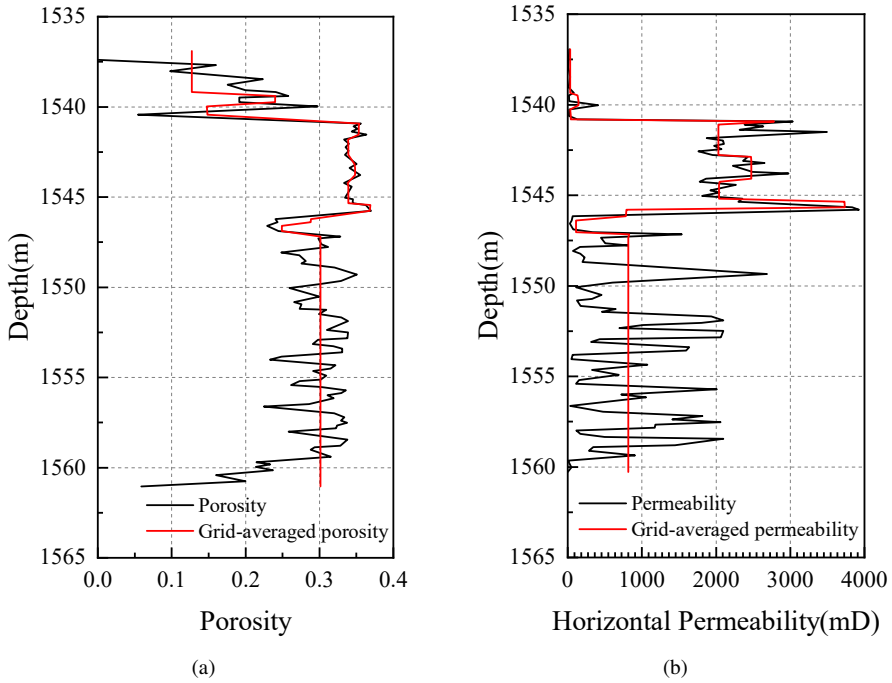

Fig. 5. Hydrogeological parameters in Frio site (Doughty et al., 2005), (a) porosity in sandstone C, (b) permeability in sandstone C.

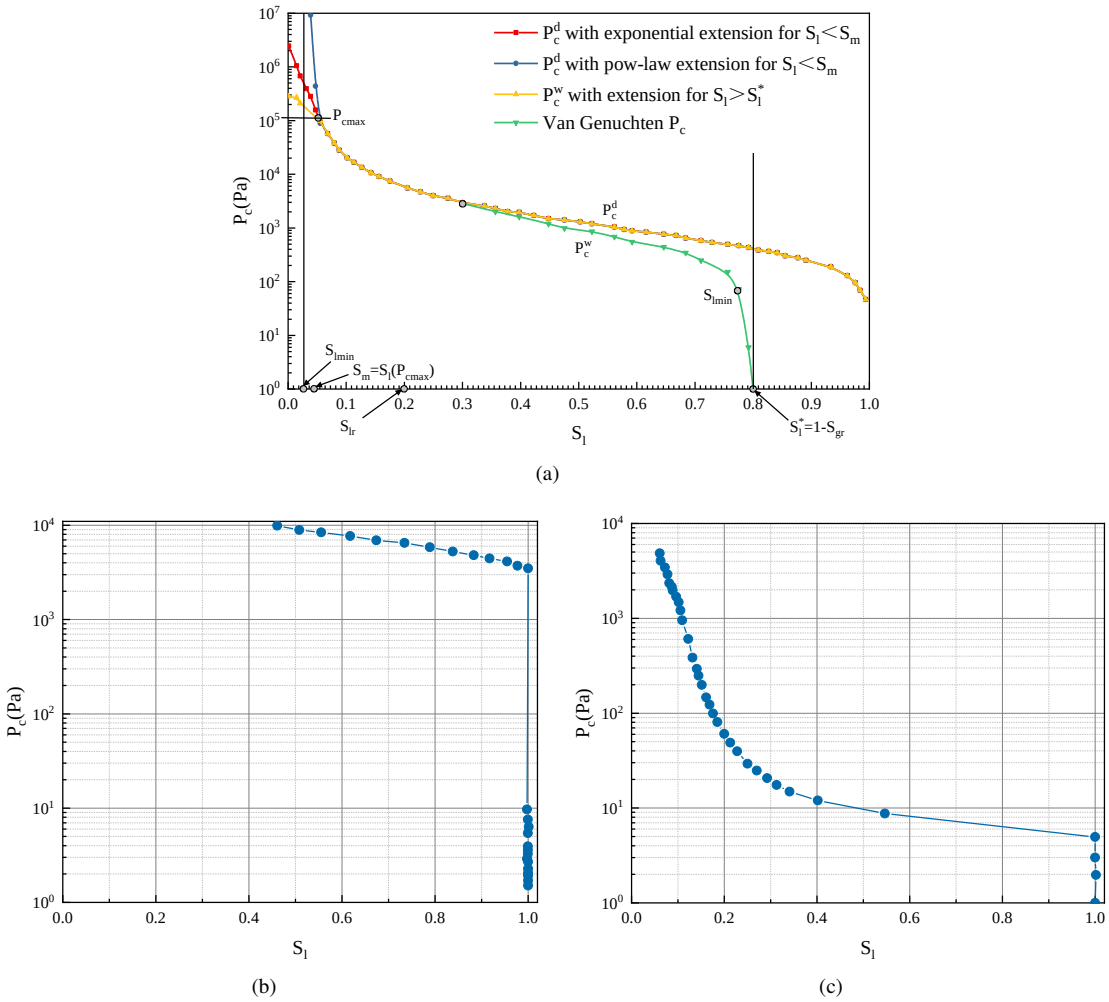

Fig. 6. Capillary pressure curves measured in sandstones and clay (Sakurai et al., 2005), (a) sandstones A and B, (b) clay, (c) sandstone C.

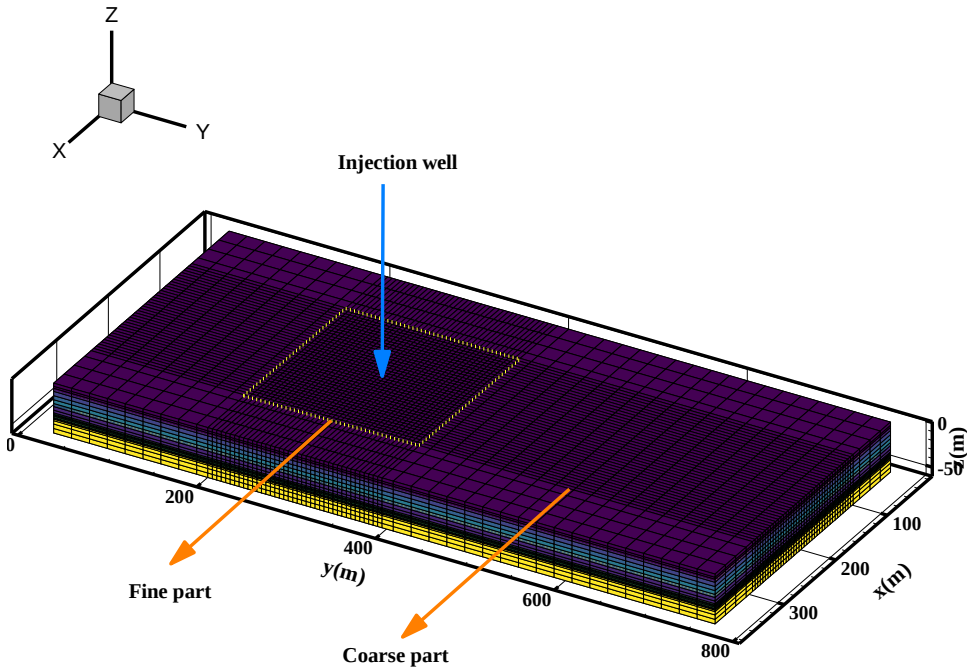

Fig. 7. Sketch diagram for 3D multiscale heterogeneous model.

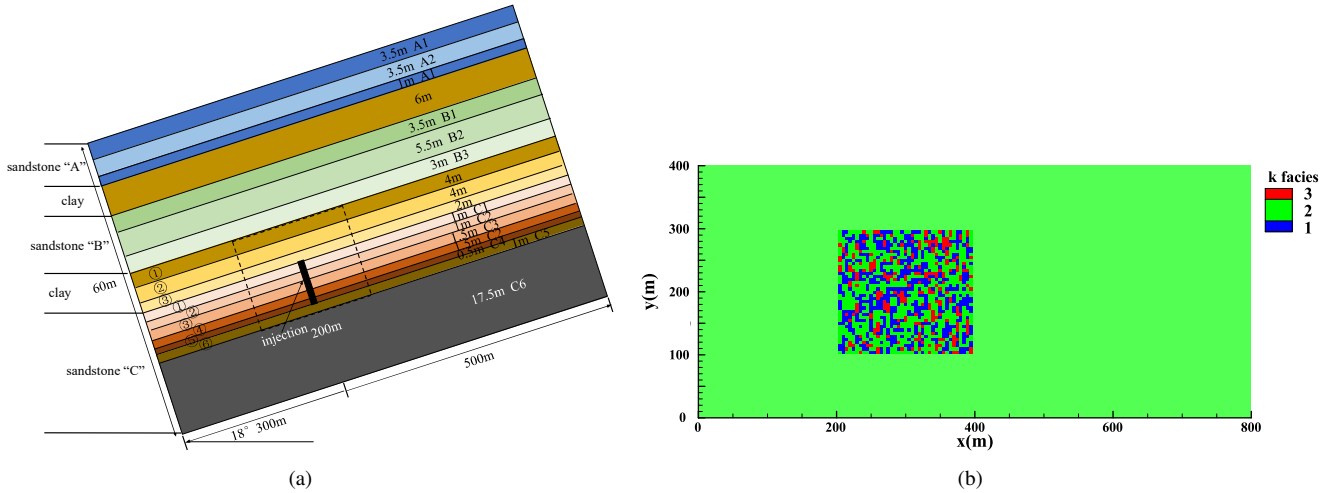

Fig. 8. Sketch diagram for multiscale model in vertical direction, (a) a multi-layer model, (b) partly fine multi-facies heterogeneous model.

the x-axis direction, the grid is divided into 50 units, of which 40 units are finely divided in 200 m area (with unit size of 5 m), and 10 units in other areas (with unit size of 20 m). Along the y-axis direction, the grid is divided into 70 units, of which 40 units are finely divided in 200 m area (with unit size of 5 m), and 30 units in other areas (with unit size of 20 m). Along the z-axis, the grid is divided into 20 units. According to the classification of lithofacies, the unit sizes from top to bottom are 3.5 m, 3.5 m, 1.0 m, 6.0 m, 3.5 m, 5.5 m, 3.0 m, 4.0 m, 2.0 m, 1.0 m, 1.5 m, 1.5 m, 0.5 m, 1.0 m, 2. 5 m, 5.0 m, 5.0 m and 5.0 m respectively. The facies distribution in some $X-Y$ and $X-Z$ cross sections are given in Sections 3.2.1 and 3.2.2.

3.2.1 Multiscale in vertical direction

In the vertical direction, a multiscale model with the dimension of 60 m $\times$ 800 m is established (as presented in Fig. 8). Firstly, a multilayer model is built up, as shown in Fig. 8(a). The sandstone layer A is divided into three sublayers with three facies, i.e., A1 (3.5 m), A2 (3.5 m) and A1 (1m). The sandstone layer B is divided into three sublayers with three facies, i.e., B1 (3.5 m), B2 (5.5 m) and B3 (3 m). As the injection well locates at the top 5.5m of the sandstone layer C, fine grids are applied in this zone. The sandstone layer C is divided into seven sublayers with six facies, i.e., C1 (1 m), C2 (1 m), C3 (1.5 m), C2 (1.5 m), C4 (0.5 m), C5 (1 m) and C6 (17.5 m). The Clay layers distribute between the sandstones layers. The injection well is 300 m away from the

left boundary of the model.

Secondly, the local 16.5 m × 200 m area near the injection well is further subdivided, as shown by the dotted line in Fig. 8(b), in order to generate a local layered structure nested with multi-facies structure. Use the method based on the transition probability theory to perform random multi-facies characterization of the layers that need to be refined (detailed in the next section), combine the random multi-lithographic layers and intercept one of the longitudinal planes to obtain the nested multi-facies structure.

3.2.2 Multiscale in layer direction

Random local multi-facies models for important layers are established, such as the clay layers, C1, C2, C3, C4 and C5 layers. These models have the dimension of 200m × 200m with an injection well in the center. The dimension of each grid block is 5 m × 5 m. The method based on transition probability theory which is introduced in Section 2 is applied here. The other domain of each layer is set by single facies, and its element dimension is 20 m × 5 m.

For the clay layer, from sublayer (1) to (3), it is divided into three facies according to the category of permeability. The lowest 88% is called facies 1, the middle 10% is called facies 2, and the highest 2% is called facies 3. Three different structures are created using a Markov Chain model and indicator simulation with quenching in T-PROGS. The facies distribution in each sublayer is shown in Fig. 9.

For the sandstone layer C, from sublayer (1) to (6), it is also divided into three facies with the category of permeability. In layer (1), the lowest 40% is called facies 1, the middle 52% is called facies 2, and the highest 8% is called facies 3. Similarly, permeability values are divided into three groups from small to large in layer (2)-layer (6) (layer (2): 35%, 47%, 18%; layer (3): 39%, 46%, 15%; layer (4): 35%, 47%, 18%; layer (5): 36%, 46%, 18%; layer (6): 36%, 50%, 14%). The Facies distribution in each sublayer is shown in Fig. 10.

3.3 Modeling approach

We use TOUGH2/ECO2N to simulate CO_2 migration and distribution in such a multiscale heterogeneous model. TOUGH2 is a numerical simulator for non-isothermal flows of multicomponent (Pruess, 1999), and ECO2N is a fluid property module for the TOUGH2 simulator that was designed for applications to geologic sequestration of CO_2 in saline aquifers (Pruess, 2005).

The total simulation time is specified as 100 days, with additional results generated at times of 10 days and 30 days. The dip of this aquifer layer is about 18°. CO_2 is injected uniformly at a constant rate of 1.85 kg/s (Corresponding to site CO_2 injection of 1,600 tons in 10 days). The top and bottom boundary of this aquifer in z-direction are no-flow boundaries. The lateral boundaries in both x-direction and y-direction are constant pressure boundaries. Main parameters in the multiscale heterogeneous model are given in Table 1.

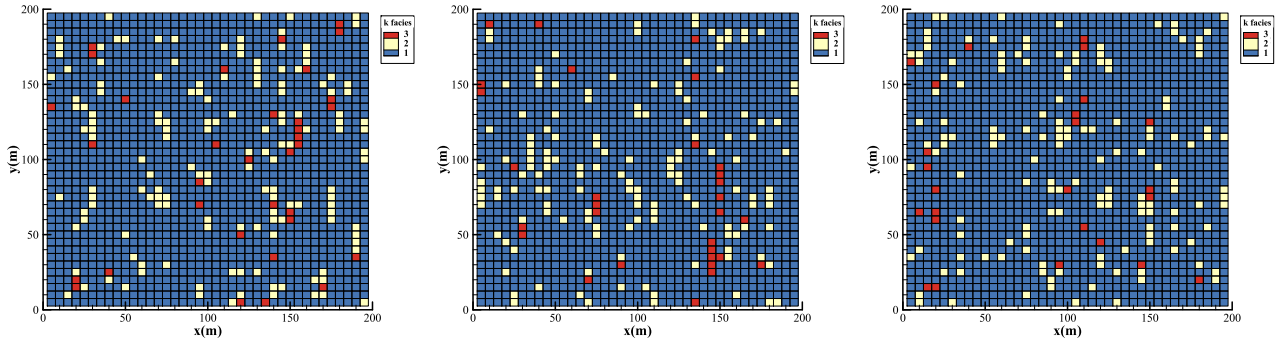

(a) (b) (c)

Fig. 9. Facies distribution for fine part in clay layers from (1) to (3), (a) facies distribution for layer (1), (b) facies distribution for layer (2), (c) facies distribution for layer (3)

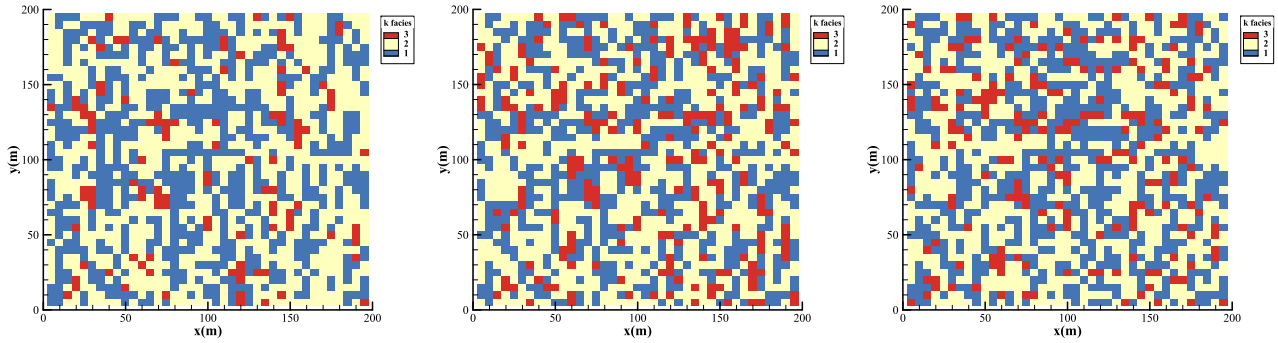

(a) (b) (c)

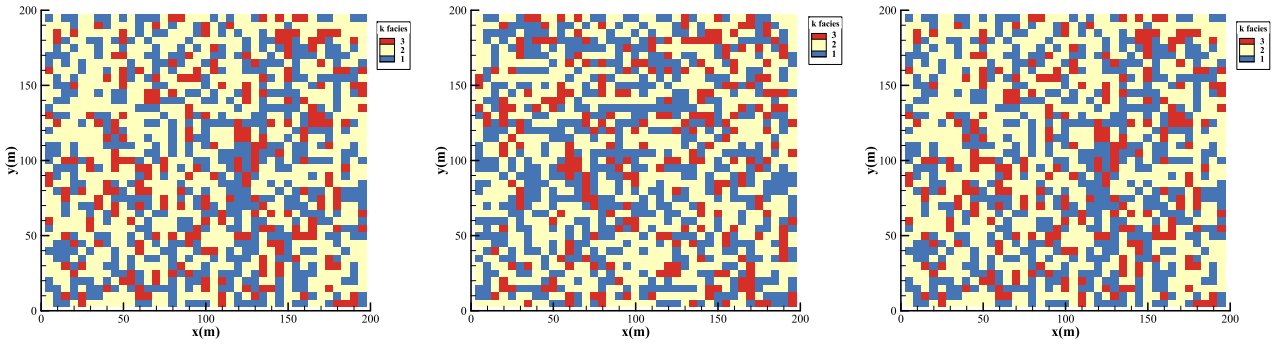

(d) (e) (f)

Fig. 10. Facies distribution for fine part in sandstone C layers from (1) to (6), (a) facies distribution for layer (1), (b) facies distribution for layer (2), (c) facies distribution for layer (3), (d) facies distribution for layer (4), (e) facies distribution for layer (5), (f) facies distribution for layer (6).

Table 1. Hydrogeologic parameters and initial conditions.

Facies (Kharaka et al., 2009)	Properties (Doughty et al., 2005)	Parameters in relative permeability function (Sakurai et al., 2005)	Parameters in capillary pressure function (Sakurai et al., 2005)	Initial conditions (Hovorka et al., 2006)
Sandstone A1	$k = 0.33$ D, $\phi = 27\%$			
Sandstone A2	$k = 0.285$ D, $\phi = 25\%$	$m = 0.457$, $S_{lr} = 0.20$, $S_{gr} = 0.20$, $S_{ls} = 1$	$m = 0.457$, $S_{lr} = 0.15$, $p_0 = 50$ Pa, $p_{\max} = 100$ kPa, $S_{ls} = 0.999$	
Sandstone B1	$k = 0.40$ D, $\phi = 26\%$			
Sandstone B2	$k = 0.358$ D, $\phi = 25\%$			
Sandstone B3	$k = 0.28$ D, $\phi = 26\%$			
Clay	$k = 0.001$ D, $\phi = 14\%$	$m = 0.557$, $S_{lr} = 0.40$, $S_{gr} = 0.05$, $S_{ls} = 1$	m=0.557, $S_{lr} = 0.35$, $p_0 = 3500$ Pa, $p_{\max} = 100$ kPa, $S_{ls} = 0.999$	$p = 15$ MPa, $T = 55\,^{\circ}$C, $S_{gas} = 0\%$, $X_{NaCl} = 3.2\%$
Sandstone C1	$k = 2.8$ D, $\phi = 35\%$			
Sandstone C2	$k = 2.0$ D, $\phi = 33\%$			
Sandstone C3	$k = 2.4$ D, $\phi = 34\%$	$m = 0.4$, $S_{lr} = 0.06$, $S_{gr} = 0.05$, $S_{ls} = 1$	$m = 0.4$, $S_{lr} = 0.05$, $p_0 = 7$ Pa, $p_{\max} = 10$ kPa, $S_{ls} = 0.999$	
Sandstone C4	$k = 3.75$ D, $\phi = 36\%$			
Sandstone C5	$k = 0.15$ D, $\phi = 25\%$			
Sandstone C6	$k = 0.8$ D, $\phi = 30\%$			

In Table 1, k[-] and ϕ[-] are the permeability and porosity of each facies type, respectively. The relative permeability and capillary pressure were to be calculated from a van Genuchten function (van Genuchten, 1980), where m[-] is the pore size distribution index for the van Genuchten model, S_{lr}[-] is residual liquild saturation, S_{gr}[-] is residual gas saturation, S_{ls}[-] is liquid saturation when liquid is saturated, p_0[-] is air entry pressure, $p_{\max}$[-] is input absolute value of maximum capillary pressure. As for the initial conditions of the formation, p[-] is pressure, T[-] is temperature (isothermal throughout), S_{gas}[-] is gas saturation, X_{NaCl}[-] is salinity of saline aquifers.

4. Results and discussion

4.1 CO_2 migration and distribution in $Y - Z$ section

Fig. 11 shows the CO_2 plume at different times in a $Y - Z$ cross section that contains the injection well. The characterization of the CO_2 plume is presented by the gas-saturation distribution.

As shown in Fig. 11, when CO_2 is injected into such a multiscale heterogeneous formation, it migrates mainly in the high permeable region, only a limit amount penetrates into the low permeable region. Since the sublayer (1) and layer (5) in the sandstone layer C are much more permeable than the other layers, the CO_2 plume presents obvious viscous fingering in the vertical direction. The phenomena occur in the initial stage of CO_2 injection, as shown in Fig. 11(a). CO_2 then migrates upward and gathers under the layer with lower permeability because of buoyancy. The shape of the CO_2 plume is similar to a funnel. In the process of upward migration, the viscous-fingering flow gradually disappears and CO_2 is trapped in local high permeable rock, as seen in Fig. 11(c). This process cannot be represented with the assumption of homogeneous formation. Values of permeability of over lain clay layer and sandstone C are quite different. CO_2 plume shows obvious viscous fingering flow in the vertical direction since the clay layers are partly finer categorized. This cannot be simulated

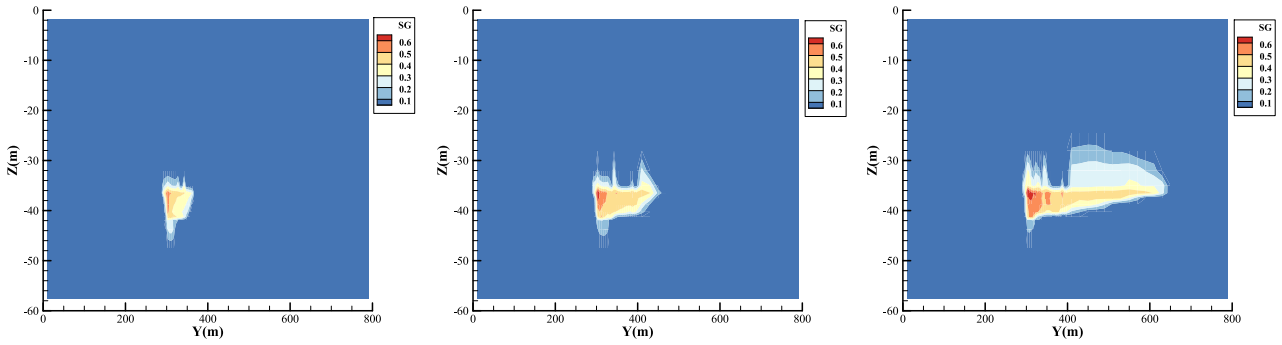

Fig. 11. Contour of gas saturation in $Y-Z$ section with injection well, (a) contour at time of 10 days, (b) contour at time of 30 days, (c) contour at time of 100 days.

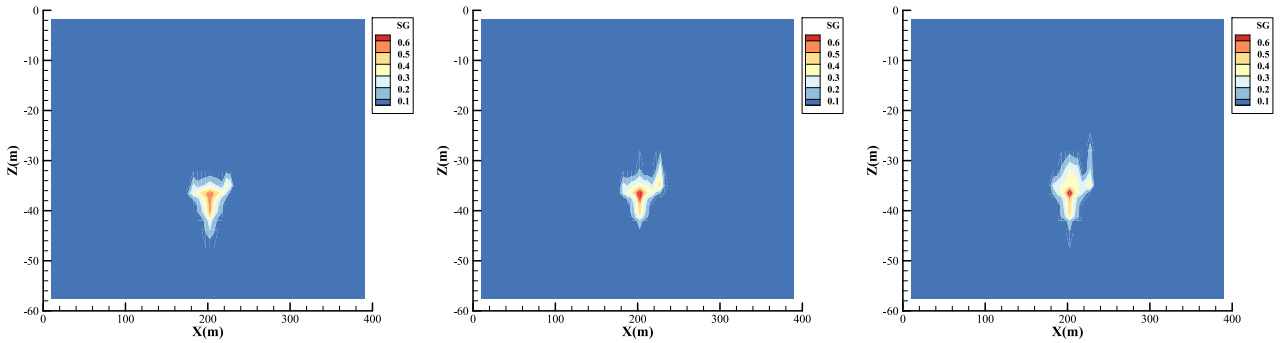

Fig. 12. Contour of gas saturation in $X-Z$ section with injection well, (a) contour at time of 10 days, (b) contour at time of 30 days, (c) contour at time of 100 days.

when a single scale is considered. Besides, the CO_2 plume distributes unevenly in a wide range due to the $Y-Z$ section has a dip of 18°, which would be different if the section is horizontal. Reservoir dip affects CO_2 migration in brine (Kumar et al., 2005).

4.2 CO_2 migration and distribution in $X-Z$ section

Fig. 12 shows CO_2 plume at different times in an $X-Z$ cross section which contains the injection well. The characterization of the CO_2 plume is presented by the gas-saturation distribution.

As time goes through, CO_2 migrates upward and collects gathers under the low-permeability layer because of buoyancy. The shape of the CO_2 plume is similar to a funnel. In the process of upward migration, CO_2 migrates advancely in a higher permeable rock. Values of permeability of over lain clay layer and sandstone C are quite different. The plume shows an obvious viscous fingering flow in the vertical direction because the clay layers are partly finer categorized. It cannot be simulated when single scale is considered.

4.3 CO_2 migration and distribution in $X-Y$ section

Fig. 13 shows CO_2 plume at different times in part of $X-Y$ sections in layer (1) and layer (5) which contains the injection well.

As shown in Fig. 13, CO_2 migrates radially in each layer from the injection well located in the center. These parts of every layer are partly multi-facies according to the finer category of permeability. CO_2 migrates advancely in higher permeable rock while penetrates little into lower permeable rock. As a result, CO_2 is trapped in local high permeable rock from 150 to 250 m in the x direction and from 300 to 400 m in the y direction, as shown in Figs. 13(a)-13(e), which show high gas saturation. It cannot be simulated when single scale is considered. Besides, CO_2 plume distributes unevenly in wide range because of buoyancy as these $X-Y$ sections have a dip of 18°. It would be different if these sections are horizontal. However, the development of deposit rocks' sediment is not horizontal in natural.

As time goes through, the CO_2 plume becomes bigger in layers (1)-(4) (as shown in Figs. 13(a)-13(c)) but smaller in layer (5). That is because the permeability of layer (5) (as shown in Figs. 13(d)-13(f)) is the highest of all these five layers, and CO_2 migrates more quickly from this layer to others under the force of buoyancy.

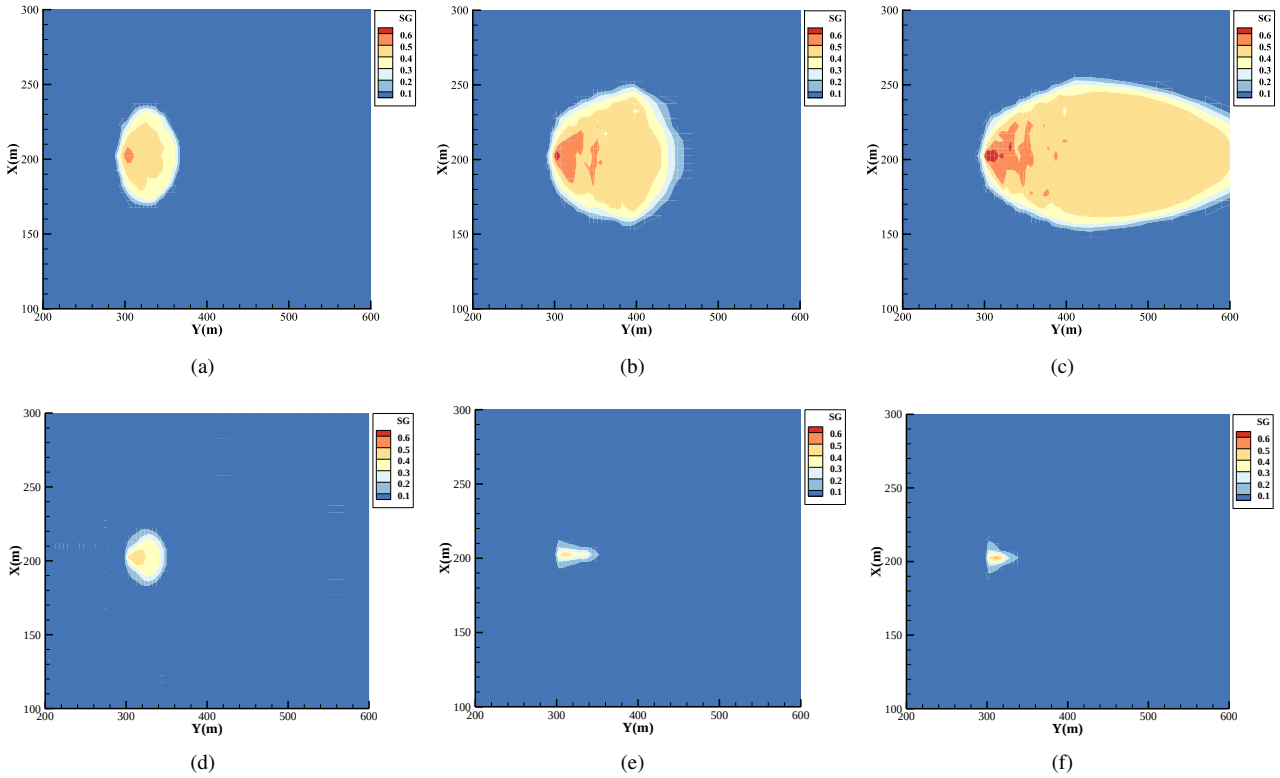

Fig. 13. (a) contour at time of 10 days in layer (1), (b) contour at time of 30 days in layer (1), (c) contour at time of 100 days in layer (1), (d) contour at time of 10 days in layer (5), (e) contour at time of 30 days in layer (5), (f) contour at time of 100 days in layer (5).

4.4 Comparison of different modeling works and seismic data

Crosswell and vertical seismic profile are adopted to monitor the CO_2 distribution using two boreholes. The purpose of the crosswell survey is to estimate the CO_2 saturation between the wells (Daley et al., 2008). Fig. 14 shows a detailed view of CO_2 saturation near the boreholes based on the crosswell survey. In this section, the important part of Fig. 11(a) is examined in detail, as shown in Fig. 15, and compare it with seismic data of the Frio situ.

Both modeling results and time-lapse tomographic imaging show that the CO_2 plume change follows the dip of the stratigraphy due to buoyancy causing up-dip migration. Fig. 14 shows an obvious velocity change on the right half of the tomogram, implies that the lower part of the plume has higher saturations. One possible reason is the presence of a low permeability zone in the center or upper part of the plume, implying vertical heterogeneity (variation in permeability or porosity). As presented in Fig. 15, our simulation results successfully captured the non-uniform migration of CO_2 in C-sand, and an obvious fingering phenomenon occurred in the lower part of the CO_2 plume. On the contrary, the traditional single-scale interlayer heterogeneity model is difficult to capture this migration feature (Fig. 16) (Doughty et al., 2008).

As shown in Fig. 16, The red line shows the location of the low vertical permeability layer that bounds the high-permeability sand above it. The CO_2 plume does not break through the top of the C-sand and not reach the low-vertical permeability layer, which is different from the observations on site (Fig. 14). As shown in Fig. 14, both the clay layer and the low permeability sandstone C layer have a small amount of CO_2 intrusion, the simulation results using the multi-scale model proposed in this paper (multi-layered heterogeneous model including multi-facies heterogeneous model) also capture this migration feature, as presented in Fig. 15.

Quantitatively, we compare the changes in saturation in the observation well (it is about 30 m away from the injection well in the Y direction in our model) calculated from the reservoir saturation tool (RST) to the modeled saturation in the same well (Fig. 17). Clearly, much better agreement was achieved between field data and our simulation results than simulation results by Ghomian et al. (2006). The maximum CO_2 saturation of the observation well is between 0.4 and 0.5. Regarding the shape of the curve, the CO_2 saturation has a double zigzag in the longitudinal direction.

5. Conclusions

In this study, a homogenous model is firstly divided into a multi-layered one with different facies categories with the spatial distribution of permeability obtained from the CCS pilot site in Frio. Then each important layer near the injection well is divided into a random multi-facies one by further assorting layered category. A method based on transition probability theory is proposed to build up the random multi-facies models. Thus, a new multiscale heterogeneous model with partly fine multi-facies heterogeneous domain is established to study CO_2 migration and distribution.

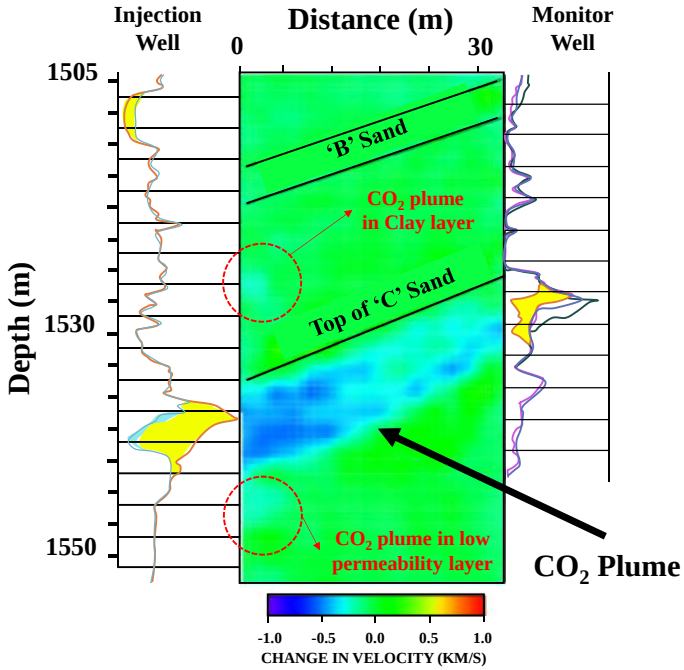

Fig. 14. Time-lapse tomographic imaging did map changes in P-wave velocity due to the CO_2 plume (modified from Daley et al. (2008)).

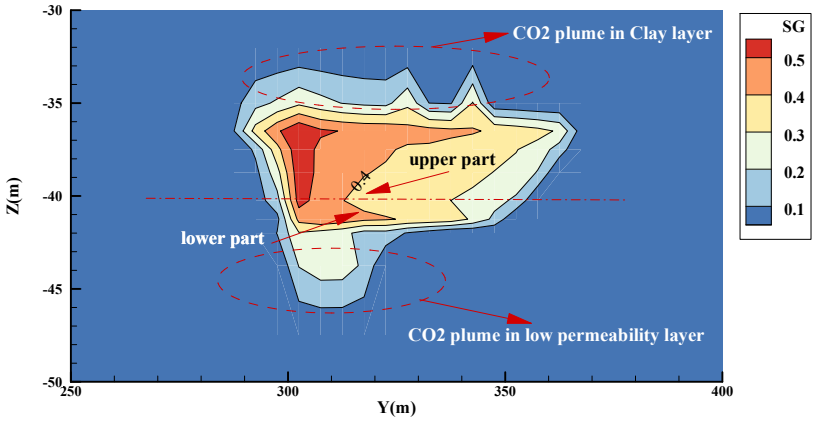

Fig. 15. CO_2 migration with numerical simulation numerical at a time of 10 days.

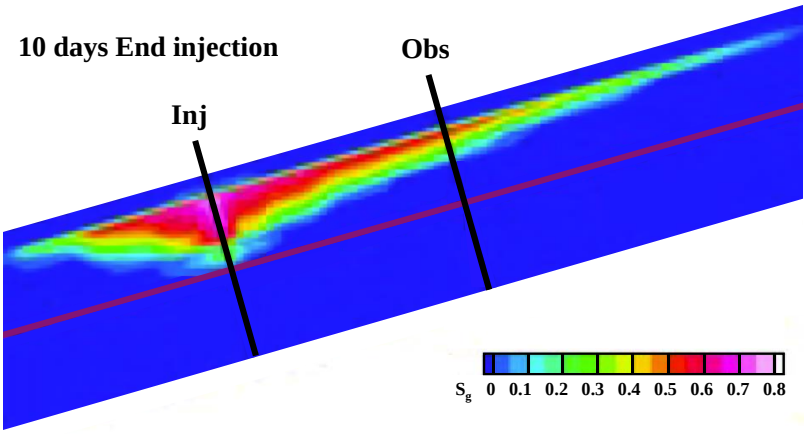

Fig. 16. Simulation results of the free-phase CO_2 plume in the vertical cross-section (Doughty et al., 2008).

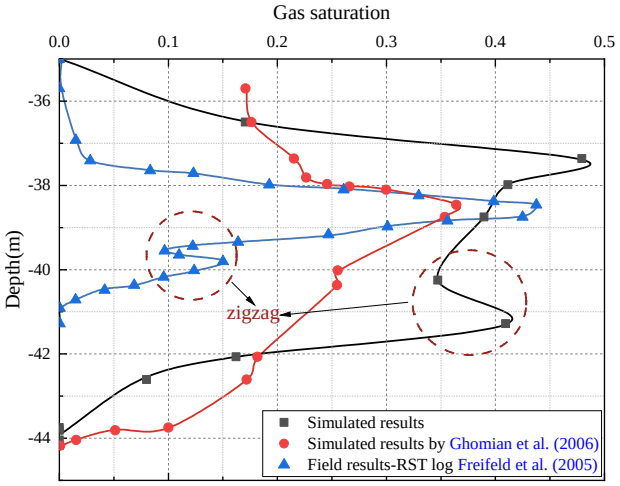

Fig. 17. Comparison of CO_2 saturation profile between values calculated from RST logs (Freifeld et al., 2005) and simulation results by Ghomian et al. (2006) and us at the observation well.

Our results show that as CO_2 is injected into such a multiscale, heterogeneous saline aquifer, on one hand, it migrates upward because of buoyancy and gathers under the layer with lower permeability. On the other hand, CO_2 migrates advance more in the high permeability region. Only a limited amount of CO_2 penetrates into the low permeability region. The CO_2 plume shows obvious viscous fingering both in layered and vertical directions. This phenomenon can not be represented with the assumption of homogeneous formation or a single-scale model is applied. Besides, the CO_2 plume distributes unevenly in a wide range because the Frio formation has a dip of 18°, which would be different if a horizontal model is used.

The results of CO_2 migration with numerical simulation at a time of 10 days are in good agreement with the seismic data in Frio situ. It proves that the new multiscale heterogeneous model with partly fine multi-facies heterogeneous domain proposed in this article can be well used to study the rules of CO_2 migration and distribution in situ. It helps forecast the front of CO_2 plume and evaluate the safety of storage.

Acknowledgement

This work was financially supported by the National Natural Science Foundation of China (No. U1765204), the Jiangsu Planned Projects for Postdoctoral Research Funds (No. 2020Z006).

Conflict of interest

The authors declare no competing interest.

References

Bachu, S., Adams, J. J. Sequestration of CO_2 in geological media in response to climate change: Capacity of deep saline aquifers to sequester CO_2 in solution. Energy Conversion & Management, 2003, 44(20): 3151-3175.

Basirat, F., Fagerlund, F., Denchik, N., et al. Numerical modelling of CO_2 injection at small-scale field experimental site in Maguelone, France. International Journal of Greenhouse Gas Control, 2016, 54(1): 200-210.

Berkowitz, B., Balberg, I. Percolation approach to the problem of hydraulic conductivity in porous media. Transport in Porous Media, 1992, 9(3): 275-286.

Birkholzer, J. T., Zhou, Q. L. Basin-scale hydrogeologic impacts of CO_2 storage: Capacity and regulatory implications. International Journal of Greenhouse Gas Control, 2009a, 3(6): 745-756.

Birkholzer, J. T., Zhou, Q. L., Tsang, C. F. Large-scale impact of CO_2 storage in deep saline aquifers: A sensitivity study on pressure response in stratified systems. International Journal of Greenhouse Gas Control, 2009b, 3(2): 181-194.

Carle, S. F. T-PROGS: Transition probability geostatistical software. University of California, Davis, 1999.

Cavanagh, A., Ringrose, P. Simulation of CO_2 distribution at the In Salah storage site using high-resolution field-scale models. Energy Procedia, 2011, 4: 3730-3737.

Daley, T. M., Myer, L. R., Peterson, J. E., et al. Time-lapse cross well seismic and VSP monitoring of injected CO_2 in a brine aquifer. Environmental Geology, 2008, 54(8): 1657-1665.

Deng, H., Stauffer, P. H., Dai, Z., et al. Simulation of industrial-scale CO_2 storage: Multi-scale heterogeneity and its impacts on storage capacity, injectivity and leakage. International Journal of Greenhouse Gas Control, 2012, 10: 397-418.

Deutsch, C. V., Journel, A. G. GSLIB: Geostatistical Software Library and User's Guide, Second Edition. Oxford, UK, Oxford University Press, 1998.

Doughty, C. Investigation of CO_2 plume behavior for a large-scale pilot test of geologic carbon storage in a saline formation. Transport in Porous Media, 2009, 82(1): 49-76.

Doughty, C., Pruess, K. Modeling supercritical carbon dioxide injection in heterogeneous porous media. Vadose Zone Journal, 2004, 3(3): 837-847.

Doughty, C., Pruess, K., Benson, S. M. Flow modeling for the frio brine pilot. Presented at Fourth Annual Conference on Carbon Capture & Sequestration. Alexandria, Virginia, 2-5 May, 2005.

Ershadnia, R., Wallace, C. D., Soltanian, M. R. CO_2 geological sequestration in heterogeneous binary media: Effects of geological and operational conditions. Advances in Geo-Energy Research, 2020, 4(4): 392-405.

Flett, M., Gurton, R., Weir, G. Heterogeneous saline formations for carbon dioxide disposal: Impact of varying heterogeneity on containment and trapping. Journal of Petroleum Science and Engineering, 2007, 57(1-2): 106-118.

Freifeld, B. M., Trautz, R. C., Kharaka, Y. K., et al. The U-tube: A novel system for acquiring borehole fluid samples from a deep geologic CO_2 sequestration experiment. Journal of Geophysical Research, 2005, 110: B10203.

Gershenzon, N. I., Ritzi Jr, R. W., Dominic, D. F., et al. Influence of small-scale fluvial architecture on CO_2 trapping processes in deep brine reservoirs. Water Resources Research, 2015, 51(10): 8240-8256.

Gershenzon, N. I., Ritzi Jr, R. W., Dominic, D. F., et al. Capillary trapping of CO_2 in heterogeneous reservoirs during the injection period. International Journal of Greenhouse Gas Control, 2017a, 59: 13-23.

Gershenzon, N. I., Ritzi Jr, R. W., Dominic, D. F., et al. CO_2 trapping in reservoirs with fluvial architecture: Sensitivity to heterogeneity in permeability and constitutive relationship parameters for different rock types. Journal of Petroleum Science and Engineering, 2017b, 155: 89-99.

Hovorka, S. D., Benson, S. M., Doughty, C., et al. Measuring permanence of CO_2 storage in saline formations: The Frio experiment. Environmental Geosciences, 2006, 13(2): 105-121.

Hovorka, S. D., Doughty, C., Benson, S. M., et al. The impact of geological heterogeneity on CO_2 storage in brine formations: A case study from the Texas Gulf Coast. Geological Society London Special Publications, 2004, 233(1): 147-163.

IPCC. IPCC special report on carbon dioxide capture and storage, Prepared by Working Group III of the Intergovernmental Panel on Climate Change. Cambridge, UK, Cambridge University Press, 2005.

Ivandic, M., Yang, C., Luth, S., et al. Time-lapse analysis of sparse 3D seismic data from the CO_2 storage pilot site at Ketzin, Germany. Journal of Applied Geophysics, 2012, 84: 14-28.

Jahangiri, H. R., Zhang, D. X. Effect of spatial heterogeneity on plume distribution and dilution during CO_2 sequestration. International Journal of Greenhouse Gas Control, 2011, 5(2): 281-293.

Kharaka, Y. K., Thordsen, J. J., Hovorka, S. D., et al. Potential environmental issues of CO_2 storage in deep saline aquifers: Geochemical results from the Frio-I Brine Pilot test, Texas, USA. Applied Geochemistry, 2009, 24(6): 1106-1112.

Koltermann, C. E., Gorelick, S. M. Heterogeneity in sedimentary deposits: A review of structure-imitating, process-imitating, and descriptive approaches. Water Resources Research, 1996, 32(9): 2617-2658.

Kumar, A., Noh, M., Pope, G. A., et al. Reservoir simulation of CO_2 storage in deep saline aquifers. SPE Journal, 2005, 10(3): 336-348.

Liu, Y. Z., Huang B. W., Wang, L. Characteristics of injection pressure and saturation distributions of supercritical CO_2 injecting into heterogeneous saline aquifers. CIESC Journal, 2010, 61(1): 32-42. (in Chinese)

Middleton, R. S., Keating, G. N., Stauffer, P. H., et al. The cross-scale science of CO_2 capture and storage: From pore scale to regional scale. Energy & Environmental Science, 2013, 5(6): 7328-7345.

Nordbotten, J. M., Celia, M. A., Bachu, S. Injection and storage of CO_2 in deep saline aquifers: Analytical solution for CO_2 plume evolution during injection. Transport in Porous Media, 2005, 58(3): 339-360.

Oruganti, Y. D., Mishra, S. An improved simplified analytical model for CO_2 plume movement and pressure buildup in deep saline formations. International Journal of Greenhouse Gas Control, 2013, 14: 49-59.

Pacala, S., Socolow, R. Stabilization wedges: Solving the climate problem for the Next 50 years with current technologies. Science, 2004, 305(5686): 968-972.

Panja, P., McLennan, J., Green, S. Impact of permeability heterogeneity on geothermal battery energy storage. Advances in Geo-Energy Research, 2021, 5(2): 127-138.

Pruess, K. ECO2N: A TOUGH2 fluid property module for mixtures of water, NaCl, and CO_2. Berkeley, Univercity of California, Lawrence Berkeley National Laboratory, 2005.

Pruess, K., Curt, O., George, M. TOUGH2 user's guide. Berkeley, Univercity of California, Lawrence Berkeley National Laboratory, 1999.

Ramanathan, R., Guin, A., Ritzi Jr, R. W., et al. Simulating the heterogeneity in braided channel belt deposits: Part 1. A geometric-based methodology and code. Water Resources Research, 2010, 46(4): 475-478.

Raza, A., Rezaee, R., Gholami, R., et al. Injectivity and quantification of capillary trapping for CO_2 storage: A review of influencing parameters. Journal of Natural Gas Science and Engineering, 2015, 26: 510-517.

Ren, J., Wang, Y., Zhang, Y. Q. A numerical simulation of a dry-out process for CO_2 sequestration in heterogeneous deep saline aquifers. Greenhouse Gases: Science and Technology, 2018, 8(6): 1090-1109.

Ronald, W. F., Lin, Z., Sally, M. B. Migration of exsolved CO_2 following depressurization of saturated brines. Berkeley, Univercity of California, Lawrence Berkeley National Laboratory, 2012.

Sahimi, M., Imdakm, A. O. Hydrodynamics of particulate motion in porous media. Physical Review Letters. 1991, 66(9): 1169-1172.

Sakurai, S., Ramakrishnan, T. S., Boyd, A., et al. Monitoring saturation changes for CO_2 sequestration: Petrophysical support of the Frio brine pilot experiment. Paper SPWLA 2005 Presented at the SPWLA 46th Annual Logging Symposium, New Orleans, Louisiana, 26-29 June, 2005.

Sardini, P., Siitari, K. M., Beaufort, D., et al. On the connected porosity of mineral aggregates in crystalline rocks. American Mineralogist. 2006, 91(7): 1069-1080.

Slatt, R. M. Stratigraphic reservoir characterization for petroleum geologists, geophysicists, and engineers. University of Oklahoma, Oklahoma, 2006.

Soeder, D. J. Greenhouse gas sources and mitigation strategies from a geosciences perspective. Advances in Geo-Energy Research, 2021, 5(3): 274-285.

Soltanian, M. R., Amooie, M. A., Gershenzon, N., et al. Dissolution trapping of carbon dioxide in heterogeneous aquifers. Environmental Science & Technology, 2017, 51(13): 7732-7741.

Soltanian, M. R., Hajirezaie, S., Hosseini, S. A., et al. Multicomponent reactive transport of carbon dioxide in fluvial heterogeneous aquifers. Journal of Natural Gas

Science and Engineering, 2019, 65: 212-223.

Soltanian, M. R., Ritzi, R. W. A new method for analysis of variance of the hydraulic and reactive attributes of aquifers as linked to hierarchical and multiscaled sedimentary architecture. Water Resources Research. 2014, 50(12): 9766-9776.

Teodoru, C. R., Prairie, Y. T., Giorgio, P. A. Spatial heterogeneity of surface CO_2 fluxes in a newly created eastmain-1 reservoir in northern quebec, Canada. Ecosystems, 2011, 14(1): 28-46.

van Genuchten, M. Th. A closed-form equation for predicting the hydraulic conductivity of unsaturated soils. Soil Science Society of America Journal, 1980, 44(5): 892-898.

Yang, Z., Chen, Y. F., Niemi, A. Gas migration and residual trapping in bimodal heterogeneous media during geological storage of CO_2. Advances in Water Resources, 2020, 142(11): 103608.

Zhou, Q., Birkholzer, J. T., Mehnert, E., et al. Modeling basin- and plume-scale processes of CO_2 storage for full-scale deployment. GroundWater, 2010, 48(4): 494-514.